

# Near-Infrared photometry of four metal-rich Bulge globular clusters: NGC 6304, NGC 6569, NGC 6637, NGC 6638 \*

E. Valenti<sup>1,2</sup>, L. Origlia<sup>2</sup>, F. R. Ferraro<sup>1</sup>

<sup>1</sup> *Dipartimento di Astronomia, Università di Bologna, Via Ranzani 1, I-40127 Bologna, Italy, e-mail elena.valenti3@unibo.it, francesco.ferraro3@unibo.it*

<sup>2</sup> *INAF-Osservatorio Astronomico di Bologna, Via Ranzani 1, I-40127 Bologna, Italy, e-mail livia.origlia@bo.astro.it*

19 November 2018

## ABSTRACT

We present high-quality near-Infrared photometry of four Bulge metal-rich globular clusters, namely: NGC 6304, NGC 6569, NGC 6637 and NGC 6638. By using the observed Colour-Magnitude Diagrams we derived a photometric estimates of the cluster reddening and distance. We performed a detailed analysis of the Red Giant Branch, presenting a complete description of morphologic parameters and evolutionary features (Bump and Tip). Photometric estimates of the cluster metallicity have been obtained by using the updated set of relations (published by our group) linking the metal abundance to a variety of near-Infrared indices measured along the Red Giant Branch. The detection of the Red Giant Branch Bump and the Tip is also presented and briefly discussed.

**Key words:** Stars: evolution — Stars: C - M — Infrared: stars — Stars: Population II Globular Clusters: individual: (NGC 6304, NGC 6569, NGC 6637, NGC 6638) — techniques: photometric

## 1 INTRODUCTION

Bulge globular clusters (GCs) are key templates of simple stellar populations to study the stellar and chemical evolution in the high metallicity domain.

A few optical and near-Infrared (IR) ground-based photometric studies of the Bulge GCs have been performed in the past decade (see e.g. Frogel et al. 1995; Ortolani, Barbuy & Bica 1996; Ortolani, Bica & Barbuy 1996; Guarnieri et al. 1998; Heitsch & Richtler 1999; Davidge et al. 1992; Momany et al. 2003). However, the relative faintness of these targets in the optical, the lack of complete and homogeneous surveys, the modest performances of the previous generation of IR arrays (i.e. limited size, large fraction of bad pixels, etc.), prevented a detailed and quantitative characterization of the Post Main Sequence (Post-MS) evolution in the high metallicity domain, as potentially traced by this GC sub-system. In this respect, the Two-Micron All-Sky Survey (2MASS) could represent a step forward but its modest spatial resolution and photometric

depth prevent to sample the cluster population with the sufficient accuracy and statistical significance, particularly in the core region.

In this framework, our group started a long-term project devoted to fully characterize the stellar populations in the Bulge GC system, by using Colour-Magnitude Diagrams (CMDs) and Luminosity Functions (LFs) in the near-IR (see Ferraro et al. 2000; Valenti et al. 2004; Valenti, Ferraro & Origlia 2004a,b; Sollima et al. 2004). As well known, in this spectral domain the reddening and blanketing effects at high metallicity are much less severe than in the optical, moreover, the sensitivity to the physical parameters of cool stars is maximum and the contrast between the red giants and the fainter MS population is greater than in any other optical passband, drastically reducing the crowding, even in the innermost core region (see e.g. Ferraro 2002, and references therein). As a first and major step forward in the study of the Bulge stellar population we are performing an homogeneous survey of a statistical significant sample of clusters in the near-IR. Such a photometric screening of the Bulge GC system with similar accuracy as that obtained for the Halo GCs system (see Ferraro et al. 2000) will allow: (i) a global check of the stellar evolution models in the high

\* Based on data taken at the ESO/NTT Telescope, within the observing programme 73.D-0313.

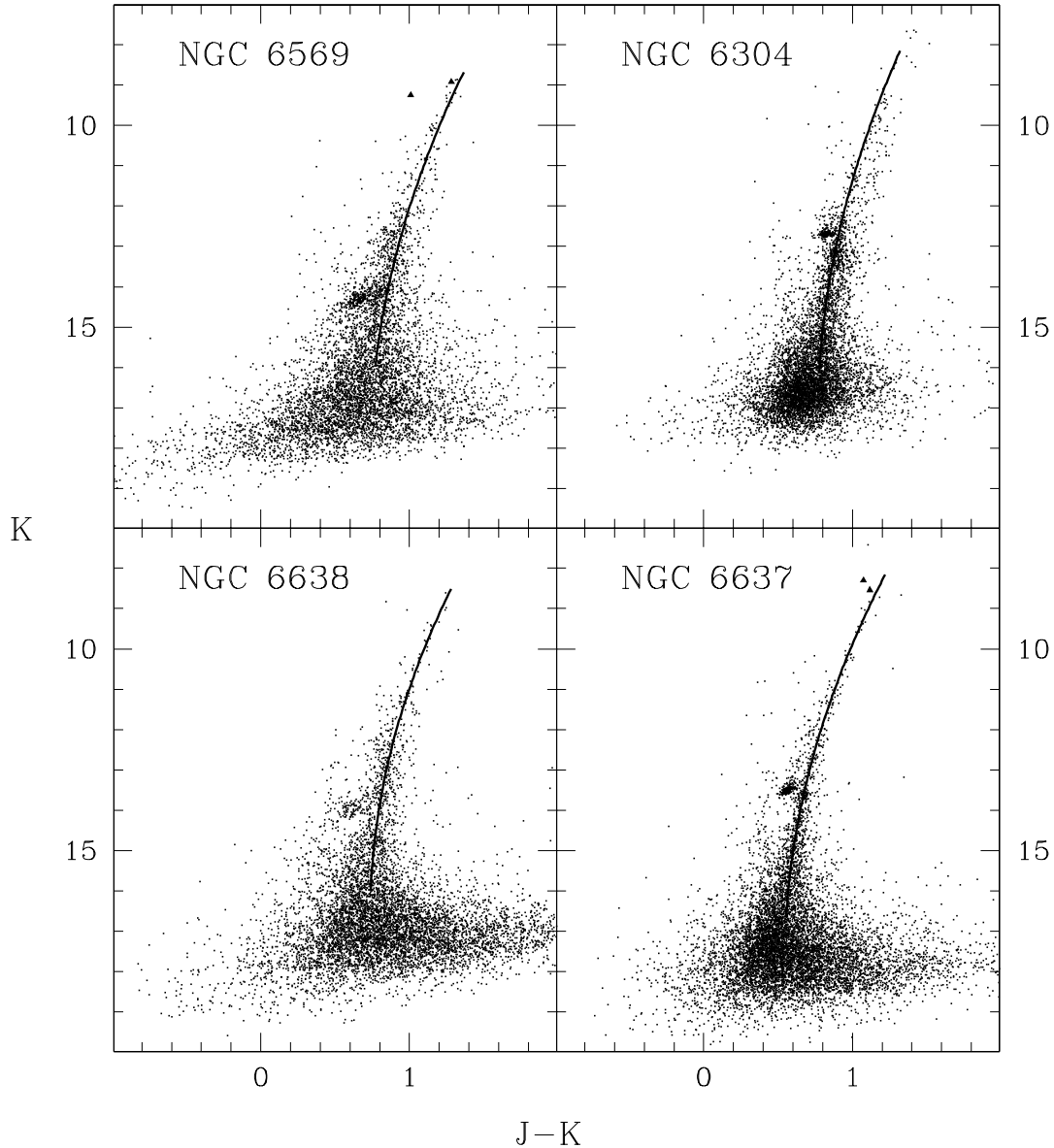


**Figure 1.** K, J-K colour-magnitude diagrams for the observed clusters. The thick line in each panel indicates the RGB fiducial ridge line. Long period variables stars have been plotted as filled triangles. Note that in the case of NGC 6304, because of bulge field contamination the RGB fiducial ridge line is referring to the dominant blue component of the cluster stellar population.

metallicity domain; *(ii)* a direct and quantitative comparison between the stellar population in the Halo and Bulge GC system; *(iii)* an accurate calibration of a few major integrated observables, to characterize the unresolved stellar populations in extragalactic bulges.

A set of near-IR photometric indices (i.e. colours, magnitudes and slopes) defined by Ferraro et al. (2000) and widely discussed in Valenti, Ferraro & Origlia (2004a,b) (hereafter *Paper I* and *Paper II*, respectively) have been derived to describe the morphology of the RGB together with

its main evolutionary features, such the RGB Bump and Tip.

In this paper we present a detailed IR study of the Red Giant Branch (RGB) sequence for a sample of four metal-rich Bulge GCs (namely, NGC 6304, NGC 6569, NGC 6637 and NGC 6638), affected by a moderate reddening  $E(B-V) < 0.6$  (see Table 2). These clusters have been subject of several studies, but mainly in the optical range; no near-IR CMDs are available for NGC 6638 and NGC 6569. Piotto et al. (2002) published B,V HST photometry of all

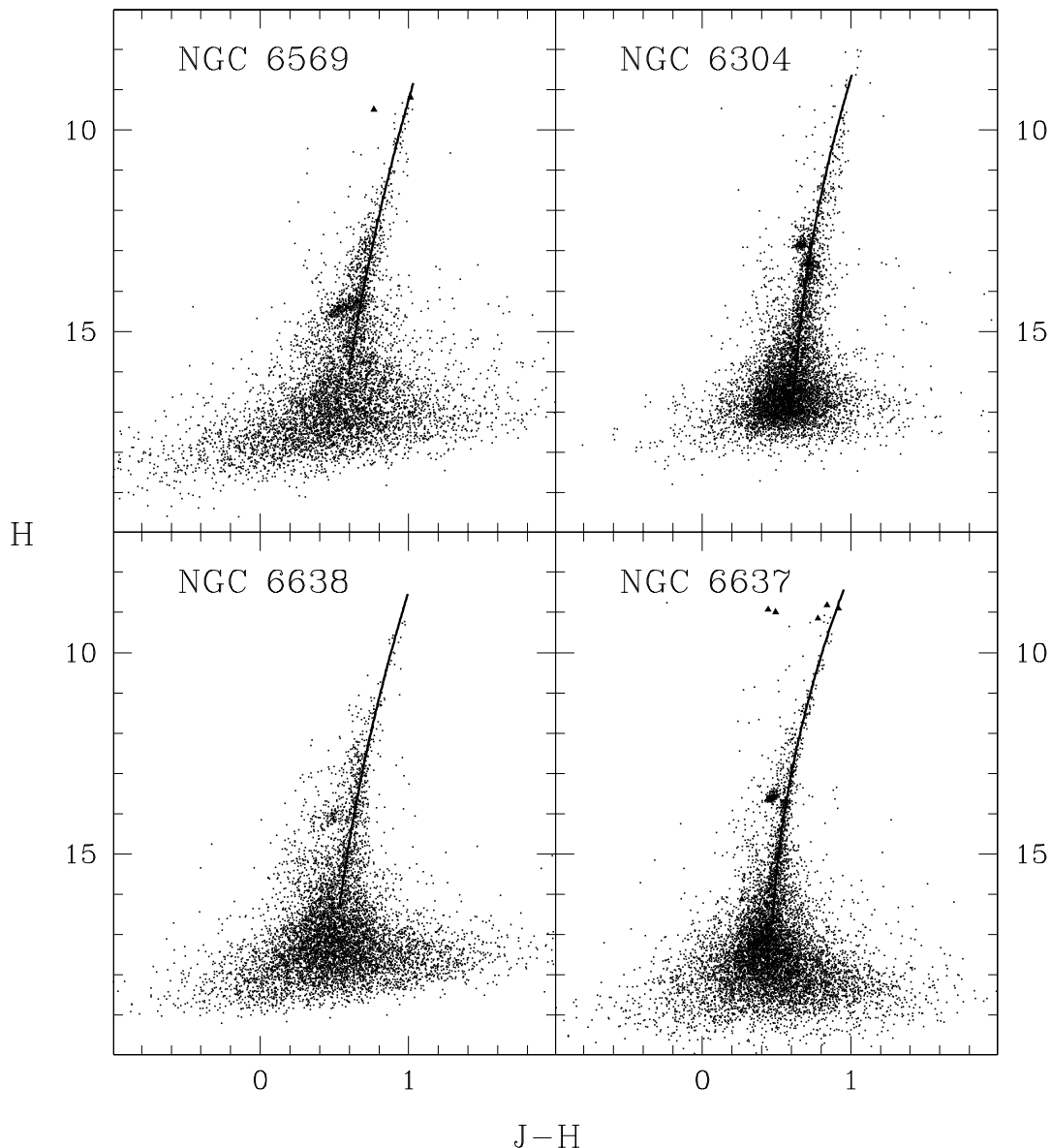


**Figure 2.** As in Fig. 1 but for the H, J-H colours-magnitude diagrams.

the programme clusters. The derived CMDs clearly show an HB morphology and a curved RGB which are typical signatures of metal-rich population; however only in the case of NGC 6637 and NGC 6304 the Sub Giant Branch (SGB) and the Turn-Off (TO) regions are well defined. V, I ground-based photometry of NGC 6304, NGC 6637 and NGC 6638 has been presented by Rosenberg et al. (2000) within a Galactic GCs survey devoted to derive the relative ages of the Milky Way GCs. However the relative high reddening and foreground contamination by MS stars, prevented a sufficiently accurate detection of the TO level. Moreover, the RGB sequence is not properly sampled and

defined. Ortolani et al. (2000, 2001) presented V,I photometry of NGC 6304 and NGC 6569, respectively, finding the presence of a red clumpy HB, a curved RGB and high level of field contamination. The advantages of observing these clusters in the near-IR has been well demonstrated by Ferraro et al. (1994) and Davidge et al. (1992) who published B,V,J,K photometry of NGC 6637 and V,K photometry of NGC 6304, respectively. The limited performances of the previous generation of IR arrays allowed only a partial sampling (both in space and deepness) of the RGB, which however is clearly defined in their observed K, V-K CMDs, thanks to the wide (V-K) spectral baseline.

In the present study, for the programme clusters we sampled the entire RGB extension in the J, H and K bands, and we presented new estimates of the reddening and distance by comparing the IR-CMDs with those of two reference clusters (47 Tuc and M 107) with well known extinction and distance modulus.

The paper is organized as follows: the observations and data reduction are presented in §2, while in §3 we describe the properties of the CMDs. §4 describes the method applied to derive an estimate of the cluster reddening and distance. In §5 we present the study of the RGB sequence: by using LFs, CMDs and RGB fiducial ridge lines, we derive the main RGB morphological and evolutionary features, and their dependences on the cluster metallicity. The results of the transformations between the observational and theoretical planes for the RGB Bump and Tip luminosities are presented in §6. Finally, in §7 we briefly summarize our results.

## 2 OBSERVATIONS AND DATA REDUCTION

A set of J, H and K images of four Bulge clusters, namely NGC 6304, NGC 6637, NGC 6569 and NGC 6638, was obtained at the European Southern Observatory (ESO), La Silla on June 2004, using the near-IR camera SOFI, mounted at the ESO/NTT telescope. During the observing runs two sets of data were secured:

(i) *Standard resolution set.* A series of images in the J, H and K bands have been obtained by using SOFI in Large mode. In this combination the camera has a pixel size of  $0''.288$  and a total field of view of  $4'.9 \times 4'.9$ . The images are the combination of 42, 72, and 99 exposures each one 3-sec long in the three pass-bands (J, H and K respectively).

(ii) *High resolution set.* High resolution images of the inner region of each cluster were also secured. The high resolution mode (SOFI coupled with the focal elongator) yields a pixel size of  $0''.146$  and a total field of view  $2'.49 \times 2'.49$ . High resolution images are the average of 30 single exposures 1.2 sec-long each.

All the secured images were roughly centered on the cluster center. Note that the region covered by our observations allows us to sample a significant fraction of the total cluster light (typically  $\sim 80\text{--}95\%$ ) in all the programme clusters. During the three nights of observation the average seeing was always quite good ( $\text{FWHM} \approx 0''.8$ ). Every image has been background-subtracted by using sky fields located several arcmin away from the cluster center, and flat-field corrected using dome flat-fields, acquired with the standard SOFI calibration setup.

Standard crowded field photometry, including Point Spread Function (PSF) modeling, was carried out on each frame by using DAOPHOTII/ALLSTAR (Stetson 1994). For each cluster, two photometric catalogues (derived from high and standard resolution images), listing the instrumental J, H and K magnitudes, were obtained by cross-correlating the single-band catalogues. The standard and high resolution catalogues have been combined by means of a proper weighted average, weighting more the high resolution measurements in the innermost region of the cluster. In principle, this strategy allows to minimize the blending effects. The internal photometric accuracy has been estimated from the rms frame-to-frame scatter of multiple stars mea-

**Table 1.** The observed sample of clusters parameters from Harris (1996) catalogue.

Name NGC	$\alpha_{2000}$	$\delta_{2000}$	l $^\circ$	b $^\circ$	$M_V$
6304	17 <sup>h</sup> 14 <sup>m</sup> 32.5 <sup>s</sup>	-29°27'44"	355.83	5.38	-7.26
6569	18 <sup>h</sup> 13 <sup>m</sup> 38.9 <sup>s</sup>	-31°49'35"	0.48	-6.68	-7.83
6637	18 <sup>h</sup> 31 <sup>m</sup> 23.2 <sup>s</sup>	-32°20'53"	1.70	-10.27	-7.47
6638	18 <sup>h</sup> 30 <sup>m</sup> 56.2 <sup>s</sup>	-25°29'47"	7.90	-7.15	-6.78

surements. Over most of the RGB extension, the internal errors are quite low ( $\sigma_J \sim \sigma_H \sim \sigma_K < 0.03$  mag), increasing up to  $\sim 0.06$  mag at  $K \geq 16$ . By using the Second Incremental Release Point Source Catalogue of 2MASS, the instrumental magnitudes were then converted into the 2MASS photometric system.<sup>1</sup>

The photometric catalogues have been also astrometrized onto 2MASS, using a procedure developed at the Bologna Observatory (P. Montegriffo, private communications) and successfully applied to other clusters (see e.g. Ferraro et al. 2003; Sollima et al. 2004, *Paper I* and *II*, and reference therein) providing rms residuals of  $\approx 0.2$  arcsec in both R.A. and DEC.

## 3 COLOUR MAGNITUDE DIAGRAMS

All stars detected over the entire science fields have been plotted in the (K, J-K) and (H, J-H) CMDs shown in Fig. 1 and 2. The main features of the CMDs are:

i) The Giant Branch is well populated in all clusters, even in the brightest magnitude bin, allowing a clear definition of the mean ridge line up to the Tip.

ii) The photometry is deep enough to reach the base of the RGB at  $K \sim H \sim 15$  mag, i.e. 3 – 4 mag below the Horizontal Branch (HB). The SGB region is not well defined, preventing any feasible detection of the Turn-Off level.

iii) The HB appears as a red clump well separated from the RGB. This is the typical morphology of high-metallicity clusters such as 47 Tuc and M 107.

iv) In the CMDs of NGC 6304, the RGB is scattered, and this is mainly due to contamination by bulge field giants (see §4.1). The blue sequence at  $(J - K) \approx 0.55$ , extending up to  $K \sim 14$  mag, corresponds to a disk MS contamination (see Ortolani et al. 2000).

v) Long Period variables have been identified, to properly locate the RGB Tip (see § 5.2).

## 4 REDDENING AND DISTANCE MODULUS

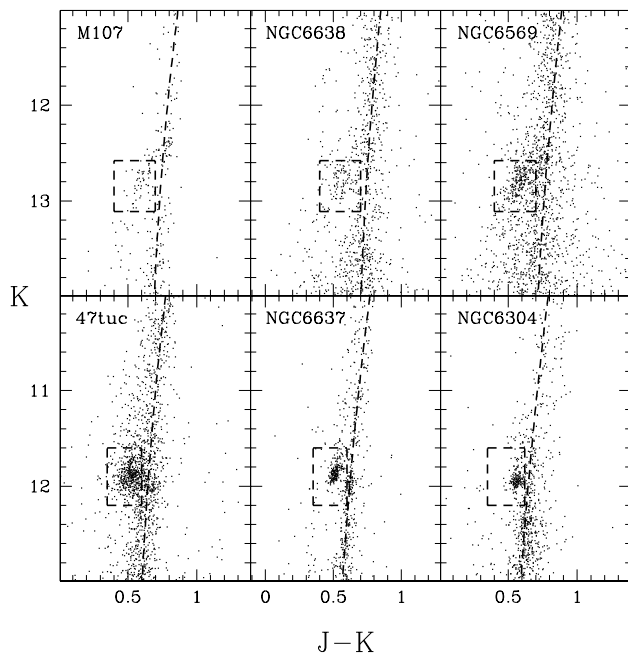
As discussed in § 2, the photometry of the four clusters presented here have been reported in the 2MASS photometric

<sup>1</sup> An overall uncertainty of  $\pm 0.05$  mag in the zero-point calibration in all three bands has been estimated. The observed cluster catalogues in the 2MASS photometric system are available in electronic form at the CDS.

**Table 2.** Metallicity, reddening and distance modulus of the programme clusters.

Name	[Fe/H] $_{Z85}^a$	[Fe/H] $_{CG97}^b$	[M/H]	E(B-V) $_{H96}$	E(B-V) $_{S98}$	E(B-V) $_{derived}$	(m-M) $_0^{H96}$	(m-M) $_0^{derived}$
NGC 6304	-0.59	-0.68	-0.55	0.53	0.52	0.58	13.90	13.88
NGC 6569	-0.86	-0.79	-0.64	0.55	0.44	0.49	15.15	15.40
NGC 6637	-0.59	-0.68	-0.55	0.16	0.17	0.14	14.78	14.87
NGC 6638	-1.15	-0.97	-0.69	0.40	0.42	0.43	14.91	15.07

Notes:

<sup>a</sup> Metallicity in the Zinn (1985) scale.<sup>b</sup> Metallicity in the CG97 scale, as computed from the Zinn (1985) estimates by using equation (7) of CG97 and following the prescription of (Ferraro et al. 1999).**Figure 3.** A zoom of the RGB at the HB luminosity level in the K, J-K plane for the programme clusters. 47 Tuc is from *Paper I*, M 107 (from Ferraro et al. 2000). The observed RGB ridge lines are shown as dashed lines, while the dashed boxes mark the HB region.

system, hence they are fully consistent with the 24 GCs published in *Paper I* and *II*. This allows to perform a detailed study of the RGB features by using the photometric indices defined by Ferraro et al. (2000) and calibrated in *Paper I* and *Paper II*. Accordingly with the assumption done in those papers, here we adopted the distance scale established by Ferraro et al. (1999), who derived the distance modulus for a sample of 61 Galactic GCs based on an empirical estimation of the Zero Age Horizontal Branch level. Here the distance modulus for the programme clusters is derived by comparing the CMDs with those of two reference clusters selected from the sample presented by Ferraro et al. (2000), and applying a differential method. As widely discussed in *Paper I*, this procedure allows to derive simultaneously distance modulus and reddening estimates. As reference clusters we adopted 47 Tuc (for NGC 6304 and NGC 6637)

and M 107 (for NGC 6569 and NGC 6638), since they have very similar metallicity and HB morphology, respectively (see Fig.3).

The differences in colours and in magnitudes between the reference and the programme clusters have been computed by shifting the CMD of each cluster to match the RGB and the HB of the reference clusters. In particular, the colour shifts ( $\delta(J-H)$  and  $\delta(J-K)$ ) have been used to derive an estimate of the relative reddening. The extinction coefficients listed by Savage & Mathis (1979) [ $A_J/E(B-V)=0.87$ ,  $A_H/E(B-V)=0.54$  and  $A_K/E(B-V)=0.38$ ] have been adopted. The results are listed in Table 2, as can be seen our reddening estimates nicely agree (within 0.1 mag) with those listed by Harris (1996) and Schlegel et al. (1998). The shifts in magnitudes ( $\delta J$  and  $\delta K$ ) once corrected for relative reddening have been used to obtain an estimate of the distance modulus for each clusters. The derived distances are listed in Table 2, column [9] and compared with those found in the Harris (1996) compilation (column [8]). Note that the distance modulus obtained here for NGC 6637 turns out to be  $\sim 0.2$  mag larger than that found by Ferraro et al. (1994). This is mainly due to a zero-point difference between the 2MASS photometric system and that adopted by Ferraro et al. (1994).

#### 4.1 The origin of the red sequence in NGC 6304

The case of NGC 6304 deserves a brief discussion since a careful examination of its CMDs has revealed the presence of a quite scattered RGB sequence (see Fig. 1 and 2). The photometric errors are not large enough to justify such a spread in colour. Moreover the same RGB morphology shown by our IR CMDs is also present in the 2MASS catalog of the same region, ruling out the possibility that the observed feature is due to any spurious effect in our photometry.

As can be clearly seen in Fig. 4, in the case of NGC 6569, NGC 6637 and NGC 6638 the (J-K) colour distribution of the RGB stars, computed in a bin of  $\sim 1.5$  mag, can be reproduced by a single Gaussian with a  $\sigma$  value compatible with the internal photometric errors. Conversely, NGC 6304 shows a colour distribution with a pronounced tail toward the red. At least two gaussian components are needed in order to reproduce the colour distribution shown in Fig. 4. The main and bluer component is representative of the cluster RGB stars, its colour distribution has in fact a  $\sigma=0.045$  comparable with those of the other clusters. A secondary

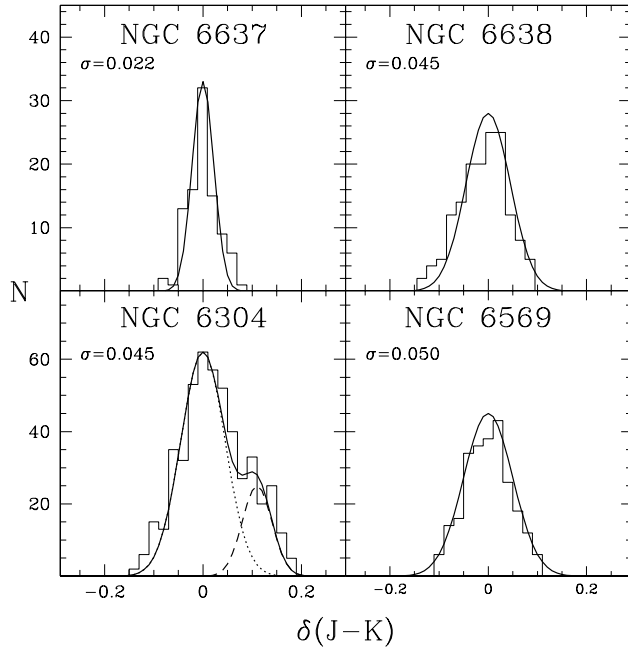


**Figure 4.** J-K Colour distribution of the RGB stars in the  $15.5 < K < 14$  magnitude range for NGC 6637 and NGC 6304 and  $12.5 < K < 11$  for NGC 6638 and NGC 6569. The solid thick lines are the Gaussian best-fits of the histograms.

component at  $\delta(J-K) \sim 0.1$  is needed in order to fit the red tail of the colour distribution (see Fig. 4). In order to check whether the red sequence could be due to field contamination, we investigated the field region around the cluster, by using 2MASS data. In particular, Fig. 5 shows the cluster CMD as obtained from our observations (panel (a)), and for comparison the CMDs of 4 control fields located at  $\sim 13'$  from the cluster center (towards North, South, East and West directions, panel (b)). As can be seen, most field giants lie on the red side of the NGC 6304 RGB. In order to make the effect more clear we divided the RGB region of the CMDs in two boxes: *Blue* and *Red Box*, respectively. As shown in the Fig. 5, the vast majority of the field RGB stars lie in the *Red Box*, while only few field giants are in the blue side of the box. To quantify the observed effect the number of field stars, per square arcmin, lying in the *Blue* and *Red Box* in bin of 1 mag has been computed. The derived density distribution is compared with the same quantity in the SOFI field. The result shown in Fig. 6, clearly indicates that almost all stars lying in the *Red Box* of panel (a) of Fig. 5 are due to Bulge field contamination (see i.e. panel (b) of Fig. 6).

Note that the same procedure has been applied to all the programme clusters. In NGC 6569, NGC 6637 and NGC 6638 the level of bulge field contamination is always less than 15%.

## 5 THE MAIN RGB FEATURES

As already discussed in detail by Ferraro et al. (2000) and *Paper I* and *II*, a complete characterization of the RGB sequence, as a function of the cluster metallicity, requires an

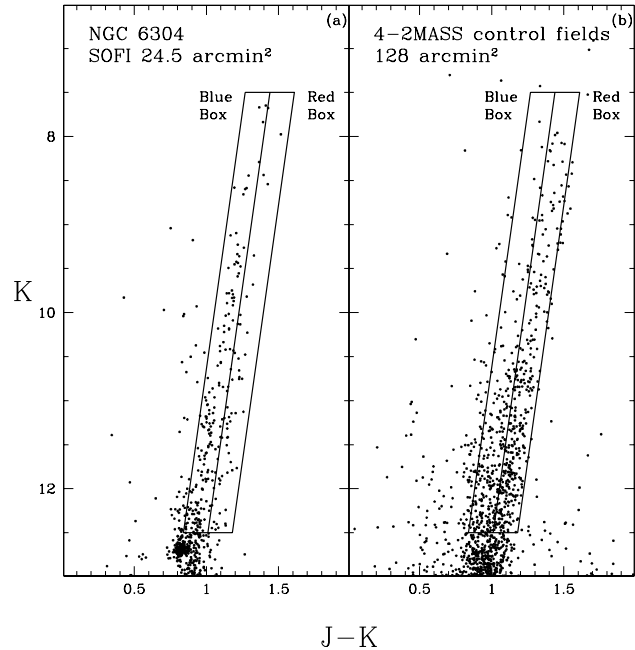


**Figure 5.** K, J-K CMDs of RGB stars detected in the SOFI field (panel (a)) and by 2MASS in 4 control fields located  $\sim 13'$  from the cluster center towards North, South, East and West directions (panel (b)).

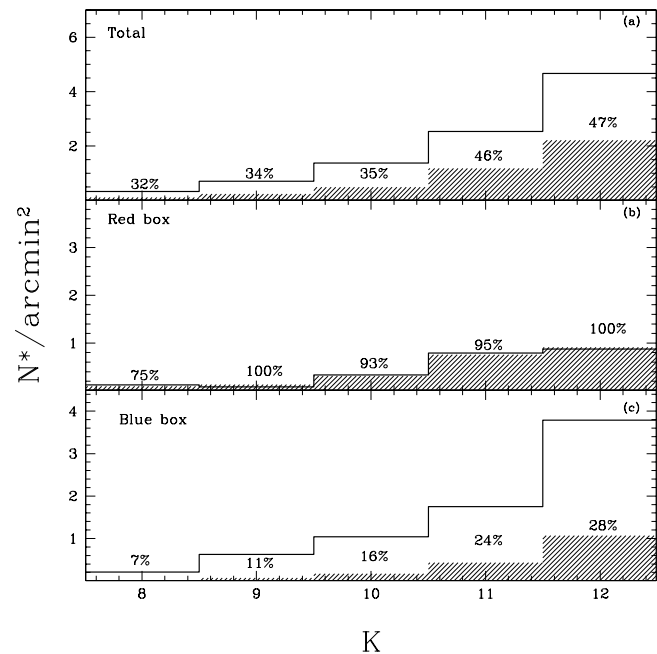


**Figure 6.** Density distribution of stars detected in SOFI (open histograms) and in 2MASS (shaded histograms) fields calculated within: both boxes (panel (a)), only the Red Box (panel (b)) and only the Blue Box. For each magnitude bin the percentage of field contamination is indicated.

**Table 3.** Adopted parameters for the observed clusters.

Name	[Fe/H] <sub>CG97</sub>	[M/H]	E(B-V)	(m-M) <sub>0</sub>
NGC 6304	-0.68	-0.55	0.58	13.88
NGC 6569	-0.79	-0.64	0.49	15.40
NGC 6637	-0.68	-0.55	0.14	14.87
NGC 6638	-0.97	-0.69	0.43	15.07
47 Tuc <sup>a</sup>	-0.70	-0.59	0.04	13.32
M 107 <sup>a</sup>	-0.87	-0.70	0.33	13.95

<sup>a</sup> From Table 2 of Ferraro et al. (1999).

appropriate definition of its morphological and evolutionary features, by using suitable CMDs and LFs. Briefly, the morphological characteristics of the RGB sequence can be obtained by computing a set of photometric indices (see §5.1) such as (i) the colours at fixed magnitudes; (ii) the magnitudes at constant colours and (iii) the RGB slope. In fact, (1) the absolute colour position, and (2) the morphology of the RGB sequence progressively change with increasing cluster metallicity. The Bump and Tip are the main RGB evolutionary features: the RGB Bump traces a significant change in the evolutionary rate of the stars along the RGB, and the RGB Tip flags the end of the RGB evolutionary phase (see §5.3).

As done in our previous studies, both the [Fe/H] in the Carretta & Gratton (1997, hereafter CG97) scale and the [M/H] global metallicity, which takes into account the contribution of the  $\alpha$ -elements, are considered. The latter has been computed by using the equation

$$[M/H] = [Fe/H]_{CG97} + \log(0.638f_{\alpha} + 0.362) \quad (1)$$

where  $f_{\alpha}$  is the enhancement factor of the  $\alpha$ -elements (i.e.  $[\alpha/Fe] \approx +0.3$  dex). Following Ferraro et al. (2000) and *Paper I* and II, an  $\alpha$ -enhancement factor linearly decreasing to zero for metal-rich clusters with  $[Fe/H]_{CG97} < -1$  have been adopted. However, it must be noted that, there is a growing number of recent high resolution spectroscopic observations of both Bulge cluster and field giants (Rich & McWilliam 2000; Carretta et al. 2001; Origlia, Rich & Castro 2002; Origlia & Rich 2004; Zoccali et al. 2004; McWilliam & Rich 2004; Origlia, Valenti & Rich 2005) which point towards a constant value of  $\alpha$ -enhancement up to solar metallicity. If a constant enhancement of  $[\alpha/Fe] \approx +0.3$  dex over the full range of metallicity is adopted, the global metallicity of the programme clusters listed in Table 3 must be increased, on average, by a few hundredths dex, the exact amount depending on their actual metallicity (the effect of such an assumption will be discussed in a forthcoming paper, Ferraro et al. 2005, in preparation).

### 5.1 The RGB morphology

In order to derive the colours at fixed magnitudes and the magnitudes at fixed colours the first step is the definition of the RGB fiducial ridge lines from the CMDs. We followed the prescriptions discussed in detail in Ferraro et al. (2000); Valenti et al. (2004). In the case of NGC 6304, where the

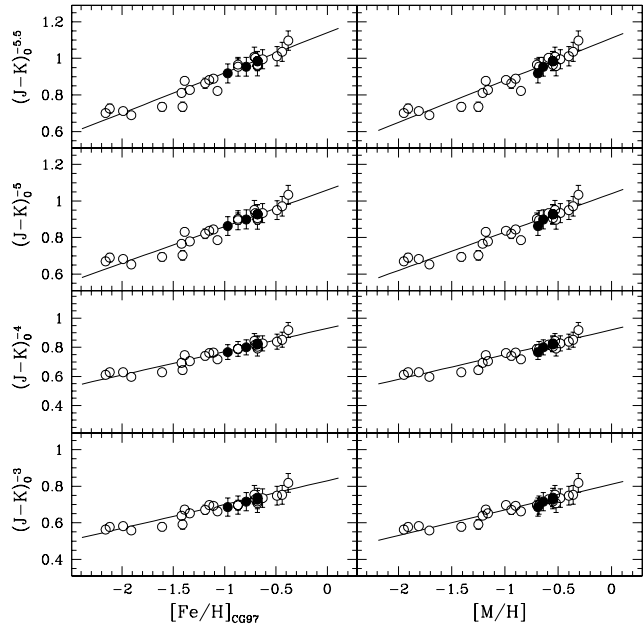


**Figure 7.** RGB mean  $(J-K)_0$  colour at fixed  $M_K = (-5.5, -5, -4, -3)$  magnitudes as a function of the CG97 metallicity scale (left panels) and of the global metallicity (right panels). Filled circles show the Bulge clusters observed here, empty circles are the clusters presented in *Paper I*. The solid lines are the calibration relations published in *Paper I*.

field contamination causes the observed splitting of the RGB sequence, the fiducial ridge line has been computed by using only the main, blue component (see § 4.1).

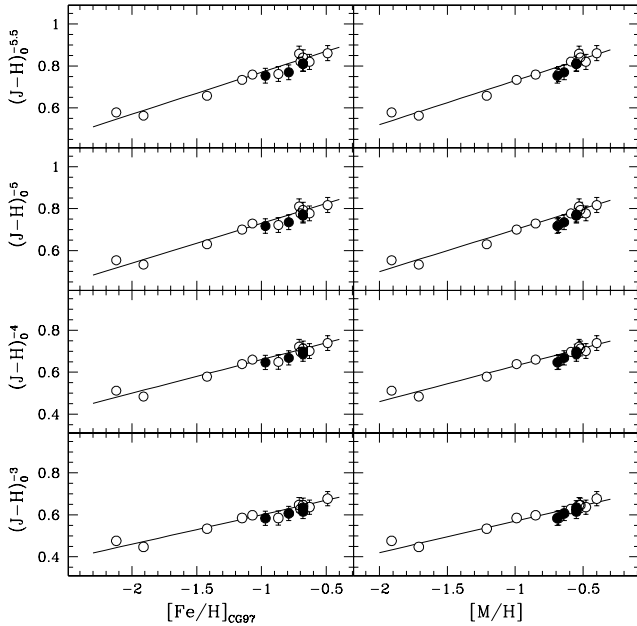
By using the values of reddening and distance modulus listed in Table 3, the observed RGB ridge lines of the programme clusters have been also converted in the absolute plane. Once obtained the intrinsic RGB ridge lines, a complete description of the RGB morphology, as a function of the cluster metallicity, follows directly.

The RGB  $(J-K)_0$  and  $(J-H)_0$  intrinsic colours corresponding to four different magnitude levels, namely  $M_{K=H} = (-5.5, -5, -4, -3)$ , as defined in Ferraro et al. (2000), are listed in Table 4, while their trends with the cluster metallicity are shown in Figs. 7 and 8, respectively. Our results nicely agree with the calibration relations (solid lines) derived in *Paper I* (see equations A1-A8 and A17-A24 in the Appendix A of *Paper I*). As expected from previous studies (Cohen & Sleeper 1995; Ferraro et al. 2000; Valenti et al. 2004, an *Paper I*), the linear scaling of the colours with the cluster metallicity is confirmed, up to the highest metallicities. Table 6 and 7 list the various photometric estimates of metallicity in both the CG97 and global metallicity scales, as computed using the relations (A1-A8 and A17-A24) of *Paper I* and the colours listed in Table 4. They are all consistent within  $\pm 0.1$  dex.

The behaviour of the RGB magnitudes at fixed colours as a function of metallicity has been investigated in all the observed clusters. Table 4 lists the derived  $M_K$  and  $M_H$  magnitudes at constant  $(J-K)_0$  and  $(J-H)_0$  colours. Fig. 9 shows how these two indices linearly correlate with the metallicity in both adopted scales. The *Paper I* sample together with

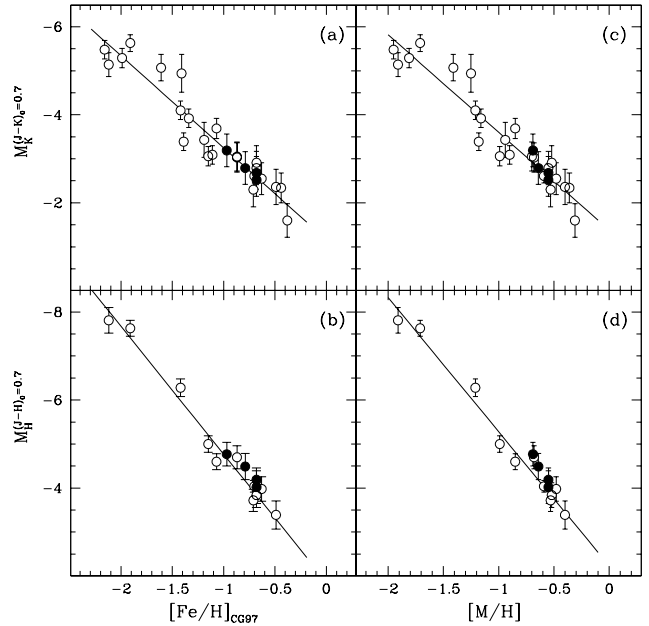
**Table 4.** Photometric indices describing the RGB location in colour and in magnitude in the K,J-K and H, J-H planes, for the observed clusters.

Name	NGC 6304	NGC 6569	NGC 6637	NGC 6638
$(J-K)_0^{M_K=-5.5}$	$0.984\pm 0.052$	$0.954\pm 0.052$	$0.986\pm 0.051$	$0.918\pm 0.050$
$(J-K)_0^{M_K=-5}$	$0.928\pm 0.052$	$0.899\pm 0.052$	$0.927\pm 0.051$	$0.863\pm 0.050$
$(J-K)_0^{M_K=-4}$	$0.827\pm 0.052$	$0.800\pm 0.052$	$0.820\pm 0.051$	$0.767\pm 0.050$
$(J-K)_0^{M_K=-3}$	$0.738\pm 0.052$	$0.716\pm 0.052$	$0.727\pm 0.051$	$0.686\pm 0.050$
$(J-H)_0^{M_H=-5.5}$	$0.812\pm 0.035$	$0.770\pm 0.035$	$0.809\pm 0.034$	$0.754\pm 0.034$
$(J-H)_0^{M_H=-5}$	$0.772\pm 0.035$	$0.735\pm 0.035$	$0.766\pm 0.034$	$0.717\pm 0.034$
$(J-H)_0^{M_H=-4}$	$0.699\pm 0.035$	$0.668\pm 0.035$	$0.686\pm 0.034$	$0.647\pm 0.034$
$(J-H)_0^{M_H=-3}$	$0.634\pm 0.035$	$0.607\pm 0.035$	$0.616\pm 0.034$	$0.584\pm 0.034$
$M_K^{(J-K)_0=0.7}$	$-2.52\pm 0.04$	$-2.79\pm 0.04$	$-2.68\pm 0.04$	$-3.19\pm 0.04$
$M_H^{(J-H)_0=0.7}$	$-4.02\pm 0.04$	$-4.49\pm 0.03$	$-4.19\pm 0.03$	$-4.77\pm 0.03$
$RGB_{slope}$	$-0.094\pm 0.005$	$-0.089\pm 0.003$	$-0.092\pm 0.003$	$-0.087\pm 0.004$

**Figure 8.** The same as Fig. 7, but for the  $(J-H)_0$  colours.

the corresponding calibration relations are also plotted. A detailed discussion on the errors associated to the derived colours and magnitudes can be found in *Paper I*. Here we just remind that, while the accuracy on the derived colours at fixed magnitudes is mainly driven by the uncertainty on the distance modulus, the errors associated on the derived magnitudes at constant colours depend on both reddening and distance uncertainty with almost the same weight. Column [4] of Table 6 and 7 lists the photometric estimate of  $[Fe/H]$  and  $[M/H]$ , respectively, derived by averaging the metallicity computed by using the relations A33&A37 and A35&A39 of *Paper I* and the absolute  $M_K$  and  $M_H$  magnitudes listed in Table 4.

Another photometric estimate of the cluster metallicity is provided by the RGB slope, which turns out to be particularly powerful being both reddening and distance indepen-

**Figure 9.** Upper panels:  $M_K$  at fixed  $(J-K)_0=0.7$  as a function of the metallicity in the CG97 scale (a) and in the global scale (c). Lower panels:  $M_H$  at fixed  $(J-H)_0=0.7$  as a function of the metallicity in the CG97 scale (b) and in the global scale (d). The filled circles refer to the present sample, the empty circles the sample of *Paper I*. The solid lines are the calibration relations derived in *Paper I*.

dent. The RGB slope in the K, J-K plane for the programme clusters have been computed following the prescriptions of *Paper I*. Photometric estimates of the clusters metallicity in both adopted scales have been obtained by using the derived RGB slope and the relations A41&A42 of *Paper I*. The results, listed in column [5] of Table 6 and 7 are fully consistent with those obtained by using the colour and magnitude photometric indices, within  $\leq 0.1$  dex.



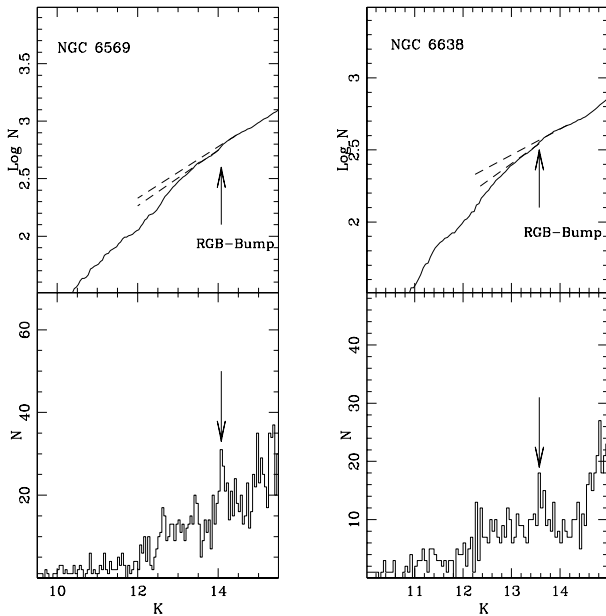


**Figure 10.** Observed integrated (upper panels) and differential (lower panels) luminosity functions for RGB stars in NGC 6569 and NGC 6638. The dashed lines in the upper panels are the linear fits to the region above and below the RGB bump.

## 5.2 The RGB evolutionary features

The RGB Bump flags the point when, during the post-MS evolution of low mass stars, the narrow hydrogen-burning shell reaches the discontinuity in the hydrogen distribution profile, generated by the previous innermost penetration of the convective envelope. The detection of the RGB Bump in Galactic and Local Group stellar systems, has been subject of many studies (see i.e. Fusi Pecci et al. 1990; Ferraro et al. 1999; Zoccali et al. 1999; Ferraro et al. 2000; Riello et al. 2003; Valenti et al. 2004; Sollima et al. 2004; Bellazzini, Ferraro & Pancino 2001; Bellazzini et al. 2002; Monaco et al. 2002, and *Paper II*), demonstrating how this feature can be safely identified by using suitable CMDs and LFs. In fact, the position of the RGB Bump corresponds to a peak in the differential LF and to a slope change in the integrated LF. Following the same procedure adopted by Ferraro et al. (2000); Valenti et al. (2004) and *Paper II*, the RGB Bump of the programme clusters has been detected in all the pass-bands. As an example, Fig. 10 and 11 show the integrated and differential LFs, in the K band, for RGB stars in all the observed clusters.

The observed J, H and K Bump magnitudes are listed in Table 5. Fig. 12 shows the behaviour of the RGB Bump absolute magnitudes as a function of metallicity in both the adopted scales. The location of the Bump in NGC 6304 is somewhat uncertain due to the bulge field contamination (see § 4.1). Indeed, the RGB-LF in this cluster shows a few, broad/asymmetric peaks, the most pronounced being about 0.3 mag fainter than the corresponding peak in NGC 6637; by assuming the same age and same helium content for the two clusters, this would imply a difference in metallicity of  $\delta[M/H] \sim 0.15$  dex.

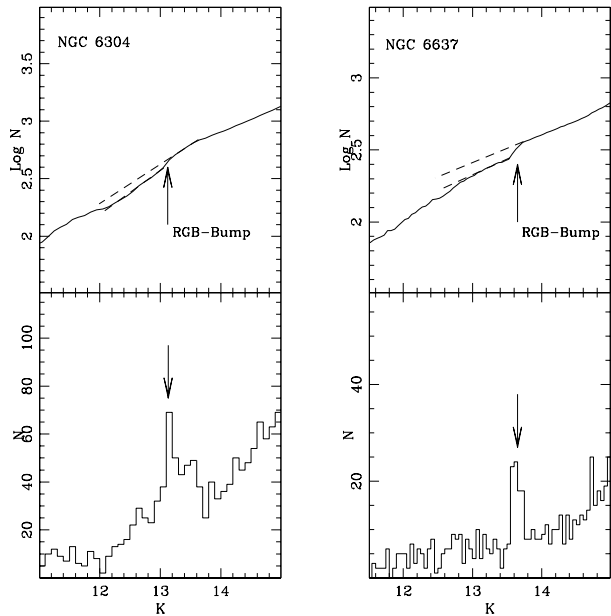


**Figure 11.** As in Fig. 10 but for NGC 6304 and NGC 6637.

By using equations 1-6 of *Paper II* linking the Bump magnitude to the cluster metal content we have also derived independent estimates of metallicity in both the adopted scales (see Table 5).

For stellar population older than  $\tau \approx 1-2$  Gyr (i.e. when stars less massive than  $M \approx 2.0 M_{\odot}$  are evolving) the RGB Tip reaches its maximum luminosity, and it remains approximately constant with increasing the population age. The calibration of the relation linking the RGB Tip magnitude to the cluster metallicity is, therefore, a fundamental step in view of using the RGB Tip luminosity as standard candle (see Bellazzini, Ferraro & Pancino 2001). In *Paper II* we recently published an updated calibration of the RGB Tip magnitudes with varying metallicity in the near-IR J, H and K bands, based on a sample of 24 Galactic GCs. Here we present the estimates of the RGB Tip luminosity for the programme clusters obtained following the same procedure adopted there. Briefly, this method is based on the assumption that the brightest non-variable star along the RGB can be considered as representative of the RGB Tip level. The presence in our IR catalogue of variable stars along the RGB has been checked by using the catalogue by Clement et al. (2001). The few variables are marked as large filled triangles in the CMDs plotted in Fig 1 and 2. The measures of the RGB Tip obtained for the programme clusters are listed in Table 5, while Fig. 13 shows the absolute RGB Tip magnitudes as a function of the cluster metallicity in both the adopted scales. As can be seen, our results nicely agree with the relations derived in *Paper II*. Note that in the case of NGC 6637, the brightest non-variable RGB star is different from that one identified by Ferraro et al. (2000) as representative of the Tip level. This is due to the fact that the star used by Ferraro et al. (2000) was a blend, which we were able to separate into two stars, thanks to the superior spatial resolution of SOFI.

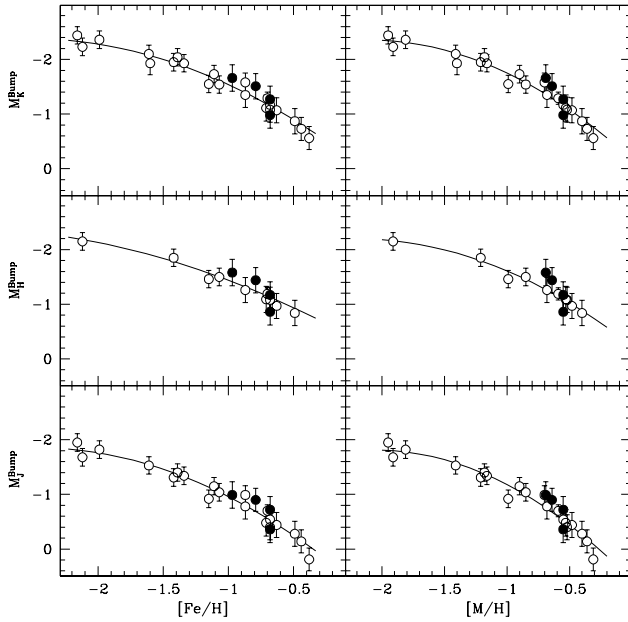


**Figure 12.** The RGB Bump absolute K, H and J magnitudes as a function of the cluster metallicity in the CG97 scale (left panels) and in the global scale (right panels). Filled circles are the programme clusters, empty circles are the *Paper II* data set. The solid lines are the calibration relations from *Paper II*.

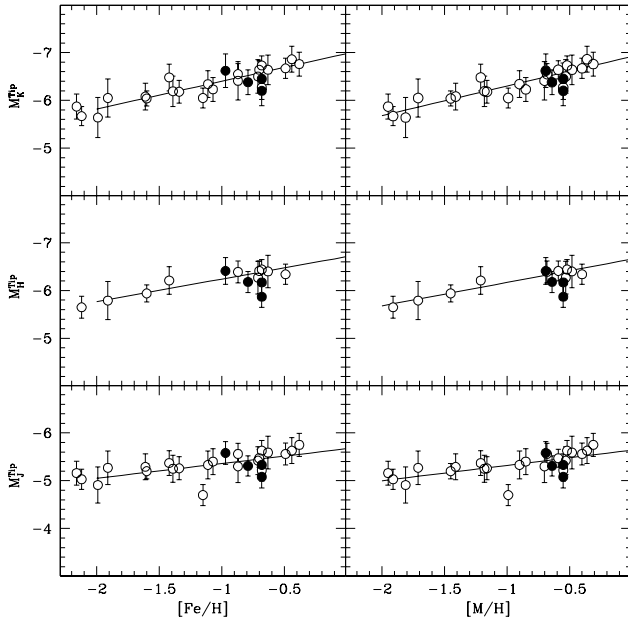


**Figure 13.** The RGB Tip absolute K, H and J magnitudes as a function of the cluster metallicity in the CG97 scale (left panels) and in the global scale (right panels). Filled circles are the programme clusters, empty circles are the *Paper II* data set. The solid lines are the calibration relations from *Paper II*.

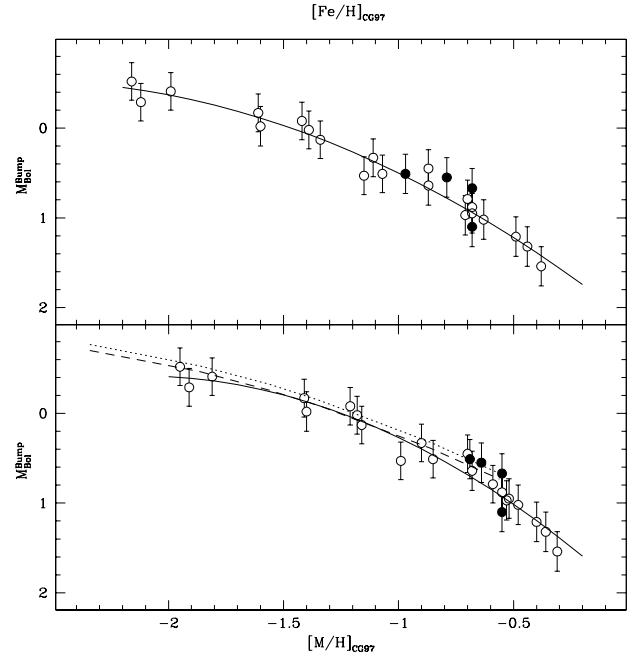


**Figure 14.** Bolometric magnitudes of the RGB Bump as a function of the cluster metallicity in both the CG97 (upper panel) and global (lower panel) scales. Filled circles show the present cluster sample and empty circles are the *Paper II* dataset. The solid lines are the calibration relations from *Paper II*, the dashed and dotted lines (lower panel) are the theoretical prediction by Straniero, Chieffi & Limongi (1997) at  $t=12$  and  $14$  Gyr, respectively.

## 6 THE THEORETICAL PLANE

In order to compare the observed RGB evolutionary features with the model predictions, it is necessary to transform the observables into the theoretical plane, by converting the absolute magnitudes into the bolometric one. In doing this, the bolometric corrections for Population II giants published by Montegriffo et al. (1998) have been used. Table 5 lists the bolometric magnitudes of both the RGB Bump and Tip for the observed cluster sample, Figs. 14,15 show their trend with the cluster metallicity in both the adopted scales. As can be seen, the values obtained for the programme clusters well fit into the relations calibrated in *Paper II*.

Theoretical predictions of the Bump features by Straniero, Chieffi & Limongi (1997) show an excellent agreement with the observations (see Fig. 14). Because of the statistical fluctuations affecting the observed RGB Tip, intrinsically poorly populated in GCs (Castellani et al. 1993), the theoretical predictions of this feature (see e.g. Caloi et al. 1997; Salaris & Cassisi 1997) have to be considered as an upper luminosity boundary to the observed values.

## 7 SUMMARY AND CONCLUSIONS

High-quality near-IR photometry of NGC 6304, NGC 6569, NGC 6637 and NGC 6638 have been presented. By using CMDs and LFs we performed a detailed analysis of the RGB morphology and evolutionary features. New estimates of the cluster distance and extinction have been obtained. A set of

**Table 6.** [Fe/H] photometric estimates for the observed clusters obtained by using the RGB morphological (colours, magnitudes and slope) and evolutionary (Bump) features.

Name	[Fe/H] <sub>CG97</sub>	[Fe/H] <sub>col</sub>	[Fe/H] <sub>mag</sub>	[Fe/H] <sub>slope</sub>	[Fe/H] <sub>Bump</sub>	<[Fe/H]>
NGC 6304	-0.68	-0.73	-0.69	-0.71	-0.55	-0.70
NGC 6569	-0.79	-0.90	-0.84	-0.82	-0.97	-0.88
NGC 6637	-0.68	-0.78	-0.76	-0.76	-0.77	-0.77
NGC 6638	-0.97	-1.06	-0.98	-0.87	-1.11	-1.00

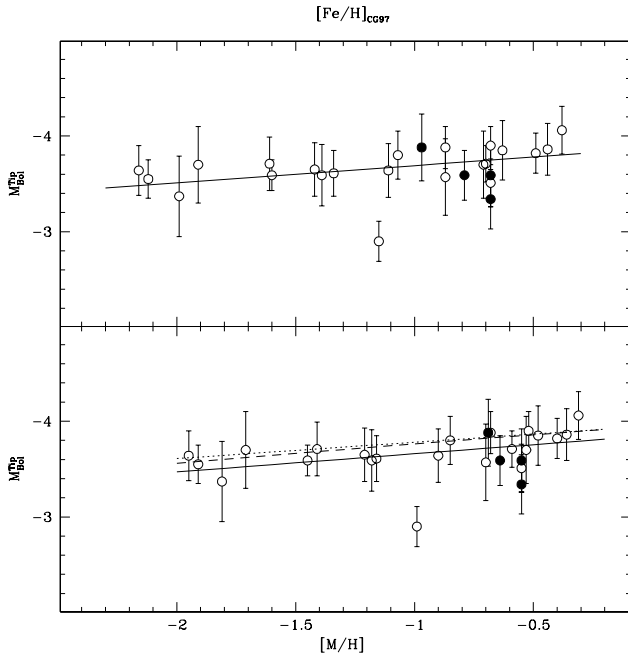


**Figure 15.** Bolometric magnitudes of the RGB Tip as a function of the cluster metallicity in both the CG97 (upper panel) and global (low panel) scales. Filled circles show the present cluster sample and empty circles are the *Paper II* dataset. The solid lines are the calibration relations from *Paper II*. Two theoretical predictions have been plotted in the lower panel: Caloi et al. (1997) (dotted line) and Salaris & Cassisi (1997) (dashed line).

**Table 5.** Near-IR and bolometric RGB Bump and Tip of the observed cluster sample.

Name	NGC 6304	NGC 6569	NGC 6637	NGC 6638
$J_{Bump}$	14.03±0.10	14.93±0.05	14.28±0.05	14.45±0.05
$H_{Bump}$	13.33±0.10	14.23±0.05	13.78±0.05	13.73±0.05
$K_{Bump}$	13.13±0.10	14.08±0.05	13.65±0.05	13.58±0.05
$J_{Tip}$	9.06±0.23	10.52±0.21	9.91±0.23	8.61±0.24
$H_{Tip}$	8.02±0.25	9.49±0.22	9.08±0.22	8.89±0.28
$K_{Tip}$	7.65±0.33	9.21±0.26	8.72±0.31	8.61±0.35
$M_{bol}^{Bump}$	1.10±0.22	0.55±0.22	0.67±0.22	0.51±0.22
$M_{bol}^{Tip}$	-3.59±0.33	-3.59±0.26	-3.34±0.31	-3.88±0.35

photometric indices has been used to provide photometric estimates of the cluster metallicity in both the [Fe/H] and [M/H] scales. We find [Fe/H]= -0.70, -0.88, -0.77, -1.00 and [M/H]= -0.54, -0.73, -0.62, -0.84 for NGC 6304, NGC 6569, NGC 6637 and NGC 6638, respectively. The Bump and the Tip bolometric luminosities are in excellent agreement with the theoretical predictions.

## ACKNOWLEDGMENTS

The financial support by the Ministero dell'Istruzione, Università e Ricerca (MIUR) is kindly acknowledged. It is a pleasure to thank the anonymous Referee for a number of useful comments which significantly improved the presentation of this work. Part of the data analysis has been performed with the software developed by P. Montegriffo at the Osservatorio Astronomico di Bologna (INAF). We thank Sergio Ortolani for making available the optical photometry of NGC 6569. We warmly thanks the ESO-La Silla Observatory Staff for assistance during the observations. This publication makes use of data products from the Two Micron All Sky Survey, which is a joint project of the University of Massachusetts and Infrared Processing and Analysis Center/California Institute of Technology, founded by the National Aeronautics and Space Administration and the National Science Foundation.

## REFERENCES

- Bellazzini, M., Ferraro, F. R., Pancino, E., 2001, ApJ, 556, 635
- Bellazzini, M., Ferraro, F. R., Origlia, L., Pancino, E., Monaco, L., Oliva, E., 2002, AJ, 124, 3222
- Caloi, V., D'Antona, F., Mazzitelli, I., 1997, A&A, 320, 823
- Carretta, E. & Gratton, R. 1997, A&AS, 12, 95 (CG97)
- Carretta, E., Cohen, J., Gratton, R.G., & Behr, B. 2001, AJ, 122, 1469
- Castellani, V., Degl'Innocenti, S. & Luridiana, V., 1993, A&A, 272, 558
- Clement, C. M., et al. 2001, AJ, 122, 2587
- Cohen, J. G. & Sleeper, C. 1995, AJ, 109, 242
- Davidge, T. J., Harris, W. E., Bridges, T. J. & Hanes, D. A., 1992, ApJS, 81, 251
- Ferraro, F. R., Fusi Pecci, F., Guarnieri, M. D., Moneti, A., Origlia, L. & Testa, V. 1994, MNRAS, 266, 829
- Ferraro, F. R., Messineo, M., Fusi Pecci, F., De Palo, A. M., Chieffi, A. & Limongi, M. 1999, AJ, 118, 1738
- Ferraro, F. R., Montegriffo, P., Origlia, L. & Fusi Pecci, F. 2000, AJ, 119, 1282

**Table 7.** [M/H] photometric estimates for the observed clusters obtained by using the RGB morphological (colours, magnitudes and slope) and evolutionary (Bump) features.

Name	[M/H]	[M/H] <sub>col</sub>	[M/H] <sub>mag</sub>	[M/H] <sub>slope</sub>	[M/H] <sub>Bump</sub>	<[M/H]>
NGC 6304	-0.55	-0.58	-0.56	-0.57	-0.44	-0.54
NGC 6569	-0.64	-0.74	-0.70	-0.68	-0.80	-0.73
NGC 6637	-0.55	-0.62	-0.62	-0.61	-0.61	-0.62
NGC 6638	-0.69	-0.90	-0.83	-0.72	-0.92	-0.84

- Ferraro, F. R. 2002, in Observed HR Diagrams and Stellar Evolution, ASP Conference Proceedings, Vol. 274. Edited by Thibault Lejeune and Joo Fernandes. San Francisco: Astronomical Society of the Pacific, 2002., p.268
- Ferraro, F. R., Possenti, A., Sabbi, E., Lagani, P., Rood, R. T., D'Amico, N., & Origlia, L. 2003, ApJ, 595, 179
- Frogel, J. A., Kuchinski, L. E. & Tiede G. P. 1995, AJ, 109,115
- Fusi Pecci, F., Ferraro, F. R., Crocker, D. A., Rood, T. R., Buonanno, R., 1990, A&A, 238, 95
- Guarnieri, M. D., Ortolani, S., Montegriffo, P., Renzini, A., Barbuy, B., Bica, E. & Moneti, A. 1998, A&A, 331, 70
- Harris, W. E. 1996, AJ, 112, 1487  
(H96), for the 2003 updated version see <http://physwww.mcmaster.ca/%7Eharris/mwgc.dat>
- Heitsch, F. & Richtler, T. 1999, A&A, 347, 455
- McWilliam, A., & Rich, R.M. 2004, Carnegie Observatories Astrophysics Series, Vol. 4: Origin and Evolution of the Elements, ed. A. McWilliam and M. Rauch (Pasadena: Carnegie Observatories, <http://www.ociw.edu/ociw/symposia/series/symposium4/proceedings.html>)
- Momany, Y., Ortolani, S., Held, E. V., Barbuy, B., Bica, Renzini, A., E., Bedin, L. R., Rich, R. M. & Marconi, G. 2003, A&A, 402, 607
- Monaco, L., Ferraro, F. R., Bellazzini, M., Pancino, E., 2002, AJ, 578, 50
- Montegriffo, P., Ferraro, F.R., Origlia, L., & Fusi Pecci, F. 1998, MNRAS, 297, 872
- Origlia, L., Rich, R. M., & Castro, S. 2002, AJ, 123, 1559
- Origlia, L., & Rich, R. M. 2004, AJ, 127, 3422
- Origlia, L., Valenti, E., & Rich, R. M. 2005, MNRAS, in press, astro-ph/0410519
- Ortolani, S., Barbuy, B. & Bica, E. 1996, A&A, 708, 733
- Ortolani, S., Bica, E. & Barbuy, B. 1996, A&A, 306, 134
- Ortolani, S., Momany, Y., Bica, E. & Barbuy, B. 2000, A&A, 357,495
- Ortolani, Bica, E. & Barbuy, B. 2001, A&A, 374, 564
- Piotto, G. et al. 2002, A&A, 391, 945
- Rich, R.M., & McWilliam, A. 2000, SPIE, 4005, 150
- Riello, M., Cassisi, S., Piotto, G., De Angeli, F., Salaris, M., Pietrinferni, A., Bono, G., Zoccali, M., 2003, A&A, 410, 553
- Rosenberg, A., Piotto, G., Saviane, I. & Aparicio, A. 2000, A&AS, 144, 5
- Salaris, M. & Cassisi, S., 1997, MNRAS, 289, 406
- Savage, B. D. & Mathis, J. S. 1979, ARA&A, 17, 73
- Schlegel, D. J., Finkbeiner, D. P. & Davis, M. 1998, ApJ, 500,525 (S98)
- Sollima, A., Ferraro, F. R., Origlia, L., Pancino, E., Bellazzini, M., 2004, A&A, 420, 173
- Stetson, P. B. 1987, PASP,99,191
- Straniero, O., Chieffi A., & Limongi, M., 1997, ApJ, 490, 425
- Valenti, E., Ferraro, F. R., Perina, S. & Origlia, L. 2004, A&A, 419, 139
- Valenti, E., Ferraro, F. R. & Origlia, L. 2004, MNRAS, 351, 1204 (*Paper I*)
- Valenti, E., Ferraro, F. R. & Origlia, L. 2004, MNRAS, 354, 815 (*Paper II*)
- Zinn, R. 1985, ApJ,293,424 (Z85)
- Zoccali, M., Cassisi, S., Bono, G., Salaris, M., 1999, AJ, 518, 49
- Zoccali, M., Barbuy, Hill, V., Ortolani, S., Renzini, A., Bica, E., Momany, Y., Pasquini, L., Minniti, D., & Rich, M. 2004, A&A, 424, 951